PHOTONICS Research

Upconversion-luminescent hydrogel optical probe for *in situ* dopamine monitoring

Bingqian Zhou,[1] Jingjing Guo,[1,2] Changxi Yang,[1] and Lingjie Kong[1,*]

[1]State Key Laboratory of Precision Measurement Technology and Instruments, Department of Precision Instrument, Tsinghua University, Beijing 100084, China
[2]e-mail: guojj018@tsinghua.edu.cn
*Corresponding author: konglj@tsinghua.edu.cn

Received 20 July 2020; revised 31 August 2020; accepted 8 September 2020; posted 8 September 2020 (Doc. ID 403223); published 30 October 2020

Dopamine (DA), as a neurotransmitter in human brain, plays a crucial role in reward motivation and motor control. An improper level of DA can be associated with neurological disorders such as schizophrenia and Parkinson's disease. To quantify DA, optical DA sensors have emerged as an attractive platform due to their capability of high-precision and label-free measurement, and immunity to electromagnetic interference. However, the lack of selectivity, limited biocompatibility, and complex fabrication processes are challenges that hinder their clinical applications. Here, we report a soft and biocompatible luminescent hydrogel optical sensor capable of recognizing and quantifying DA with a simple and compact interrogation setup. The sensor is made of a hydrogel optical fiber (HOF) incorporated with upconversion nanoparticles (UCNPs). DA molecules are detected through the luminescence energy transfer (LET) between the UCNPs and the oxidation products of DA, while the light-guiding HOF enables both excitation and emission collection of the UCNPs. The hydrogel sensor provides an optical readout that shows a linear response up to 200 μmol/L with a detection limit as low as 83.6 nmol/L. Our results show that the UCNP-based hydrogel sensor holds great promise of serving as a soft and biocompatible probe for monitoring DA *in situ*.

https://doi.org/10.1364/PRJ.403223

1. INTRODUCTION

Dopamine (DA) is a central monoamine neurotransmitter involved in the regulation of a wide range of complex processes, including normal brain function, emotions, muscle movement, and hormones [1–3]. High levels of DA in the brain are responsible for reward and pleasurable feelings, whereas its deficiency can lead to stress, depression, and motor disorders. Impaired DA transmission is associated with many neurological diseases, including epilepsy, drug addiction, memory loss, schizophrenia, Parkinson's disease, attention deficit hyperactivity disorder, and psychiatric problems [4,5]. In addition, recent studies have shown that DA concentrations in tumor tissues are usually lower than those in normal tissues [6]. Therefore, the development of efficient approaches for quantitative measurement of DA should facilitate diagnosis and treatment of neurodegenerative disorders and cancers in clinics.

To date, several methods have been developed for DA detection, including microdialysis [7], liquid chromatography (HPLC) [8], electrochemistry [9–13], colorimetry, and luminescent spectroscopy techniques [14–20]. Microdialysis and HPLC have long been the gold standard for quantitative measurement of DA but suffer from the limitations of complicated instrumentation and high cost. Fast-scan cyclic voltammetry (FSCV), one of the most popular electrochemical methods, has been successfully utilized to quantify DA with high temporal resolution and sensitivity that, however, has difficulties in distinguishing DA from other competing species of similar oxidation potential. Despite the recent progress achieved in improving the selectivity of electrochemical methods, they are still limited to a few electroactive species [21]. Luminescent and colorimetric probes such as upconversion nanoparticles (UCNPs) and quantum dots (QDs) have also shown great potential in detecting DA because of their high sensitivity and selectivity [22–25]. However, these methods require the nanoprobes to be dispersed in the analyte sample for the subsequent fluorescence analysis, which suffers from sample contamination and is susceptible to environmental interference. An attractive alternative for the design of DA sensing probes is to use functionalized optical fibers due to their miniaturized size, low cost, remote sensing capability, and electromagnetic interference (EMI) immunity [26–30]. For example, Agrawal *et al.* demonstrated an optical fiber probe functionalized with silver nanoparticles and polyethylene glycol (PEG) for DA detection based on the localized surface plasmon resonance (LSPR) effect [26]. Kim *et al.* proposed a miniaturized and

wireless optical neurotransmitter sensor by coating an optical fiber tip with modified QDs for real-time DA sensing [29]. However, optical fiber sensors using conventional optical materials such as silica and plastics are generally rigid and fragile, making them incompatible with the soft and elastic biological tissues [31–33]. To address these problems, soft and implantable optical waveguides made from polymer hydrogels such as polyacrylamide (PAAm), poly-(ethylene glycol) diacrylate (PEGDA), and agarose, have been developed with favorable optical and physio-mechanical properties for light delivery in deep tissues [34–38]. In particular, there have also been efforts in integrating photonic functions into hydrogel waveguides for biosensing (e.g., glucose monitoring [37], metal ion sensing [38,39], and toxicity detection [40]) and photomedicines [41–43]. It is highly desirable to fabricate a hydrogel optical fiber (HOF) platform that is capable of quantitative and selective monitoring of DA *in situ* while integrating high softness and biocompatibility.

Herein, we report a soft and biocompatible HOF sensor utilizing lanthanide (Ln^{3+})-doped UCNPs for quantitative and selective detection of DA. The UCNPs synthesized with a core of $NaYF_4$:Yb, Tm and a shell of $NaYF_4$ ($NaYF_4$:Yb, Tm@$NaYF_4$) are immobilized in the HOF through precursor doping. A DA molecule consists of two hydroxyl groups and one amino group, and its spontaneous oxidation produces DA quinone species (ox-DA). The ox-DA has a broad absorption peak, which overlaps with the emission peak of the UCNPs. Under near-infrared (NIR) excitation, the UCNPs generate 450 nm emissions, and the luminescence intensity is selectively quenched by DA based on luminescence energy transfer (LET) between them [23]. The HOF, capable of efficient light guiding, is made from transparent biocompatible PEGDA hydrogels, which enables facile excitation and emission collection of the UCNPs as well as endows the sensor with high mechanical compliance and biosafety. Systematic characterizations are performed, where the UCNPs-incorporated HOF (UCNPs-HOF) sensor shows a linear response to DA over the range of 0–200 μM (1 M = 1 mol/L) with detection limit as low as 83.6 nM. Furthermore, the UCNPs doped in HOF exhibit a high photostability even when immersed in aqueous samples of various pH values and temperatures, suggesting their high robustness to environmental disturbances. We show that the hydrogel optical sensor could be used as a point-of-care sensing probe for quantitative and *in situ* monitoring of DA, which could find useful applications in clinical analysis and diagnosis of DA-associated diseases.

2. EXPERIMENTAL SECTION

A. Fabrication of the UCNPs-HOF Sensor

The $NaYF_4$:Yb, Tm@$NaYF_4$ UCNPs are synthesized via the solvothermal method [44] and the obtained UCNPs, dispersed in deionized (DI) water, are used for sensor fabrication. The sensor is made of a PEGDA hydrogel fiber doped with UCNPs. The UCNPs/PEGDA hybrid precursors are prepared by mixing UCNPs (0.1% w/v) with degassed solutions of 40% w/v PEGDA (700 Da, Sigma-Aldrich) and 1% w/v 2-hydroxy-2-methyl-propiophenone (Sigma-Aldrich) in DI water. The UCNPs-HOF is fabricated by injecting the prepared precursor into a polyethylene tube mold (inner diameter, 1 mm) through a syringe and curing by ultraviolet (UV) exposure (365 nm, 5 $mW \cdot cm^{-2}$) for 5 min. For laser excitation and emission collection, a silica multimode fiber (MMF) (core/cladding, 200/215 μm) is coupled to the UCNPs-HOF by inserting the MMF tip into the center of the precursor-containing mold prior to UV curing. Afterwards, the UCNPs-HOF pigtailed with MMF is extracted out of the mold by water pressure.

B. Equipment and Characterization

The microscopic images of the UCNPs are taken by a 120 kV transmission electron microscope (Tecnai Spirit). The upconversion luminescence (UCL) emissions of the UCNPs under 980 excitation are measured by a CCD spectrometer (Thorlabs, CCS100), which has a scanning wavelength range of 350–700 nm, fully covering the UCL spectrum. Energy-dispersive X-ray (EDX) analysis of the UCNP samples is performed with an energy-dispersive spectrometer (Oxford Instruments). Statistical size distribution of the UCNPs is obtained from 200 UCNPs. Absorption spectroscopy is carried out with a UV-Vis spectrophotometer (Agilent 8453) to measure the absorption spectra of UCNPs-PEGDA hydrogels and DA samples. Temperature dependence of the UCNPs-HOF sensor is investigated by using a heating water bath equipped with a thermocouple (resolution, 0.1°C) for temperature calibration. For pH characterization, Tris-HCl (Sigma-Aldrich) and Tris base (Sigma-Aldrich) are used to prepare pH buffer solutions (ionic strength = 150 mM) with pH ranging from 4.5 to 10.5.

C. Experimental Setup for DA Detection

A fiber-coupled laser diode at 980 nm is employed to interrogate the UCNPs-HOF sensor through a 50:50 fiber coupler and MMF. The excited UCL emission is collected and guided to a portable spectrometer (Thorlabs, CCS100) for spectral analysis. A short-pass optical filter with cut-off wavelength of 850 nm is utilized to remove the residual excitation light in front of the spectrometer. Tris-HCl buffer solution (pH = 8.4, ionic strength = 150 mM) is used to prepare DA samples with concentrations ranging from 0 to 200 μM. For DA sensing, the UCNPs-HOF sensor is immersed in aqueous DA samples, and the corresponding changes in UCL spectra are continuously recorded by the spectrometer.

3. RESULTS AND DISCUSSION

DA-sensitive lanthanide (Ln^{3+})-doped UCNPs, capable of converting NIR radiation into short-wavelength visible emissions, are synthesized as the sensing components. The UCNPs are made up of an active core of $NaYF_4$:Yb, Tm and an inert shell of $NaYF_4$. Transmission electron microscopy (TEM) observation of the UCNPs shows uniform and monodisperse particles [shown in Fig. 1(a)]. The size distribution of the UCNPs taken from the TEM is fitted by a Gaussian function, indicating an estimated size of 37.86 nm [shown in Fig. 1(b)]. The composition of the UCNPs is analyzed by energy-dispersive X-ray analysis (EDXA), which confirms the elemental existence of Na, Y, F, Tm, and Yb [shown in Fig. 1(c)]. Figure 1(d) shows the schematic diagram of the

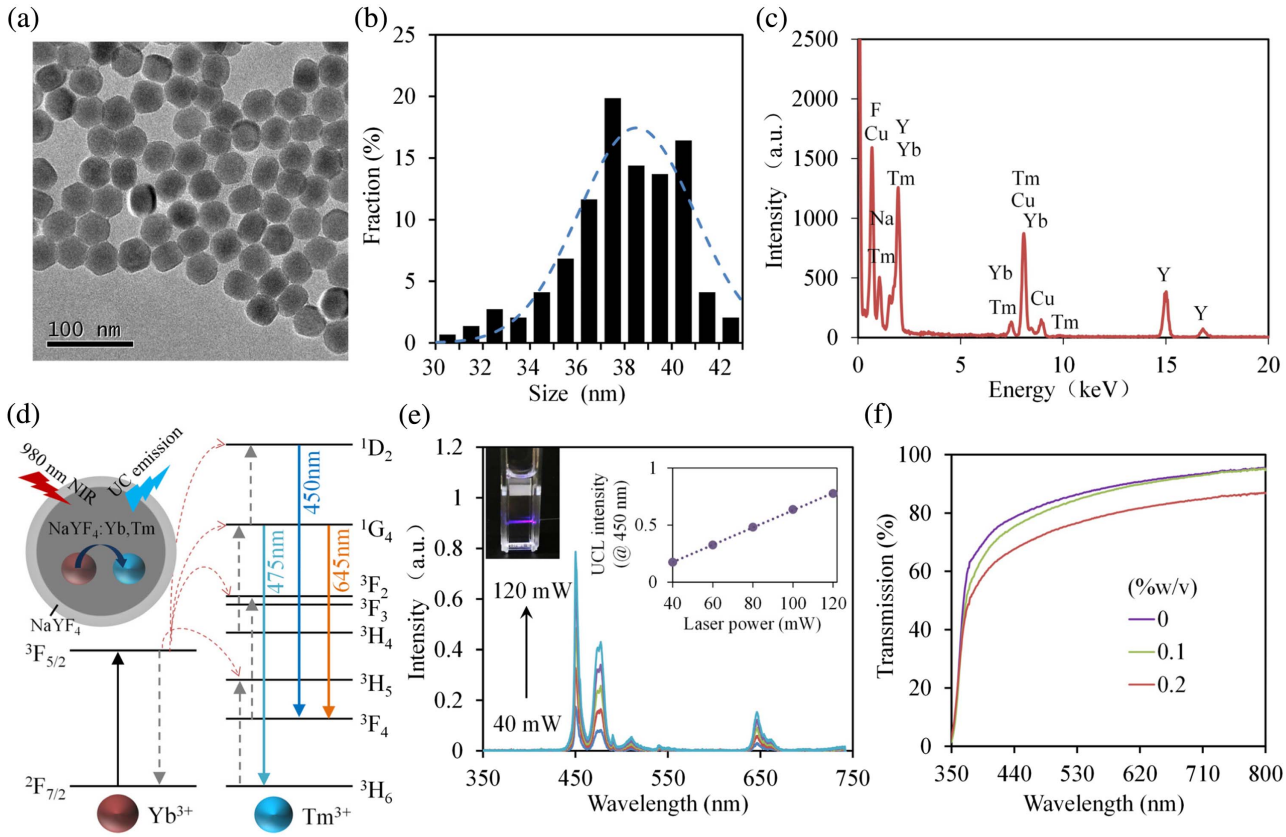

Fig. 1. (a) TEM images, (b) size distribution, (c) EDXA, and (d) schematics and upconversion process of the UCNPs. (e) Emission spectra of the UCNPs dispersed in water under different excitation powers. The concentration of the UCNPs is set at 0.1% w/v. The inset graph shows a linear relationship between emission intensity and excitation laser power. (f) Transmission spectra of hydrogel incorporated with various concentrations of UCNPs.

upconversion process of the $NaYF_4$:Yb, Tm@$NaYF_4$. While the core of $NaYF_4$:Yb, Tm provides visible emissions under 980 nm excitations via energy transfer from the Yb^{3+} ions to Tm^{3+} ions, the inert shell of $NaYF_4$ serves as a protecting layer that improves the UCL [45]. Figure 1(e) shows the UCL spectra of the aqueous UCNPs sample, where three distinct emission bands centered at 450, 475, and 645 nm are observed, corresponding to the $^1D_2 \rightarrow {}^3F_4$, $^1G_4 \rightarrow {}^3H_6$, and $^1G_4 \rightarrow {}^3F_4$ transitions of Tm^{3+}, respectively [23]. When the excitation power is increased from 40 to 120 mW, a linear increase in the peak emission intensities (@ 450 nm) of UCNPs is observed.

The synthesized UCNPs are assembled into biocompatible PEGDA hydrogels to fabricate the HOF sensor through precursor doping and UV-induced polymerization. PEGDA hydrogels are soft and biocompatible polymers that are widely used in biosensing and biomedicine [46,47]. In addition to their excellent physio-mechanical properties, PEGDA hydrogels are highly transparent in a broad spectral range, favorable for optical sensing. The pore size of 700 Da PEGDA hydrogels is less than 2 nm, and thus the large-size UCNPs could be effectively immobilized within the hydrogel matrix through physical entrapping. Absorption spectroscopy is employed to investigate the effect of the doping UCNPs on the optical transparency of the hydrogels [shown in Fig. 1(f)]. The UCNPs/PEGDA hydrogels show decreased transparency with the increasing concentrations of UCNPs, ascribed to the increased light scattering and absorption. As the doping concentration increases to 0.2% w/v, the light transmission at 450 nm decreases to nearly 60%. To achieve high light-guiding efficiency, we choose 0.1% w/v UCNPs to fabricate the UCNPs-HOF in the following experiments.

A simple molding process is employed to fabricate the UCNPs-HOF from the hybrid precursors of UCNPs and PEGDA, as depicted in Fig. 2(a). For light coupling, a silica multimode fiber (MMF) is inserted into the tube mold and aligned to its central axis prior to UV curing. To confirm its light-guiding capability, green laser light at 532 nm is launched into the UCNPs-HOF [shown in Fig. 2(b)]. The UCNPs-HOF can effectively guide light even when tied into knots, demonstrating excellent optical performance and mechanical flexibility [shown in Fig. 2(c)]. When illuminated by NIR laser at 980 nm, blue UCL emission is observed along the UCNPs-HOF as a result of the upconversion process in the incorporated UCNPs [shown in Fig. 2(d)].

Using the UCNPs-HOF as a DA sensing probe, we develop a compact optical setup for the sensor interrogation, as shown in Fig. 2(e). A 980 nm laser (~60 mW) is launched into the

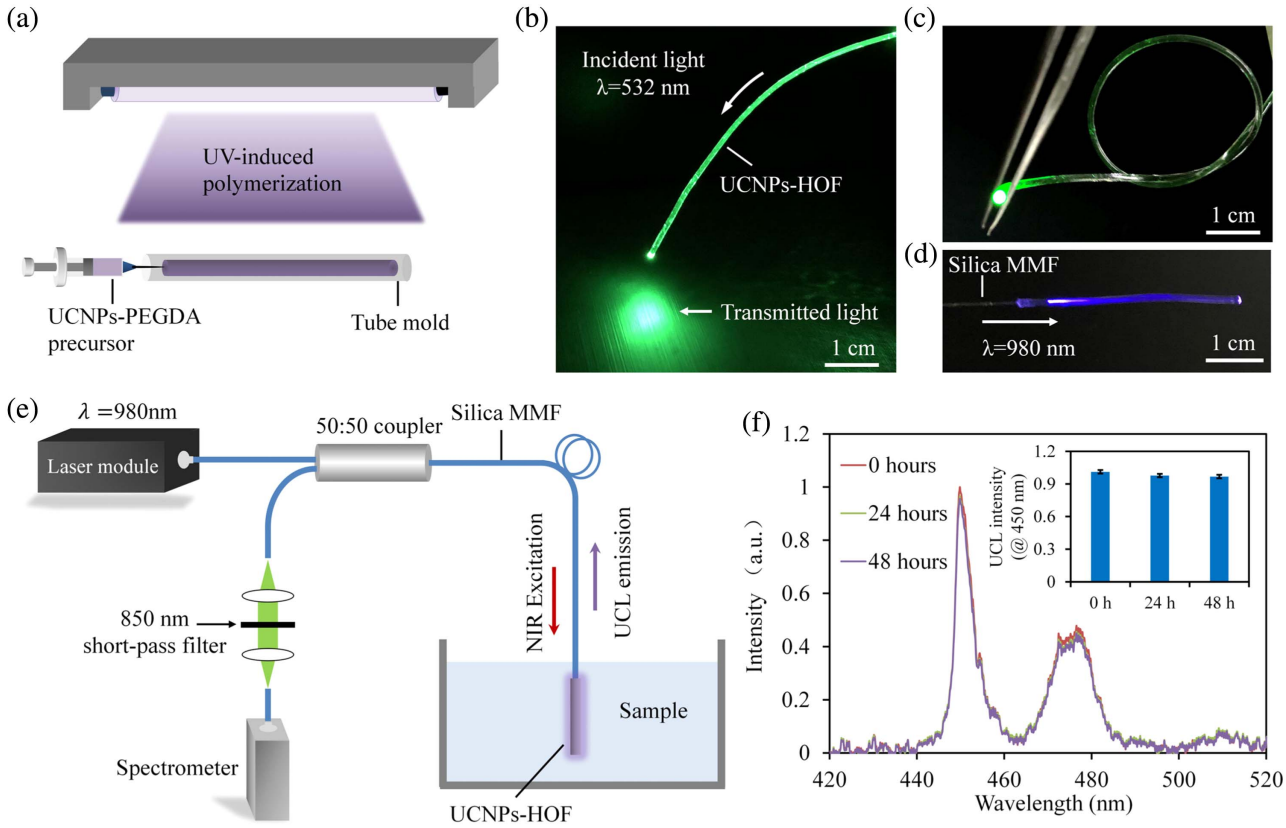

Fig. 2. (a) Fabrication of the UCNPs-HOF by molding and UV-induced crosslinking. (b) Coupling of a 532 nm laser to the UCNPs-HOF. (c) Mechanical flexibility. The UCNPs-HOF can effectively guide light even when tied into a knot. (d) Photograph showing blue UCL emission of the UCNPs-HOF under the illumination of an excitation laser at 980 nm. (e) Optical setup for interrogation of the sensing UCNPs-HOF. (f) Long-term stability.

sensing fiber through a 50:50 fiber coupler and MMF, and the UCL emission is guided to a spectrometer for spectral analysis. The UCNPs-HOF is immersed in aqueous samples at room temperature, during which its emission spectrum is continuously recorded. To confirm the immobilization of UCNPs in the HOF, the UCL emission spectrum is continuously monitored for 48 h [shown in Fig. 2(f)]. Negligible changes are observed in the UCL intensities, suggesting excellent photo-stability and no leakage of UCNPs from the hydrogel matrix.

For implantable sensing applications, temperature and pH are important factors to be considered since body temperature highly fluctuates over time, and the pH values of various biological samples (such as blood, urine, or cerebrospinal fluid) may differ greatly. For accurate sensing, it is essential to develop a DA sensor that is insensitive to changes of temperature and pH. As such, we investigate the dependence of the UCL intensities of the UCNPs on pH and temperature. Figure 3(a) shows the UCL spectra of the sensor when immersed in a Tris-HCl buffer solution (pH = 8.4, ionic strength = 150 mM) at various temperatures. The UCL intensity maintains good stability, with a maximum fluctuation of 6.5% in the temperature range of 29–52°C, fairly large to cover the variation of normal body temperature [shown in Fig. 3(b)]. Figure 3(c) shows the UCL intensities of the sensing fiber in buffer solutions with pH ranging from 4.6 to 10.6, demonstrating that the UCL intensity is insensitive to the changes of pH.

The mechanism of the UCNPs-HOF sensor for DA sensing is based on the quenching effect of the UCNPs towards DA [shown in Fig. 4(a)]. The design of HOF enables not only fast exchanges with the surrounding analytes but also efficient light confinement for high signal-to-noise ratio (SNR) [38]. The oxidation of DA molecules yields ox-DA, which has a broad absorption peak overlapping the emission peak of UCNPs around 450 nm [shown in Fig. 4(b)]. Thus, the energy created by NIR excitation of the donor UCNPs is reabsorbed by the acceptor ox-DA, resulting in UCL quenching [23]. Selectivity of a specific biosensor is crucial for practical applications due to potential presences of other interfering species. To investigate the selectivity of the UCNPs-HOF sensor to DA, the sensor is tested with aqueous samples separately containing DA, $CaCl_2$, KCl, NaCl, glycine (Gly), L-glutamate (L-Glu), glucose (GLU), uric acid (UA), ascorbic acid (AA), and S-adenosylmetionine (SAM), which are commonly present in human biofluids [shown in Fig. 4(c)]. The quenching ratios (I_0/I) of the UCNPs-HOF sensor towards DA samples are much higher than those of other samples, which are close to 1 [shown in Fig. 4(d)]. The high selectivity of the UCNPs-HOF sensor for DA detection is attributed to the specific emission–reabsorption mechanism, making it robust against potential coexistence of other species.

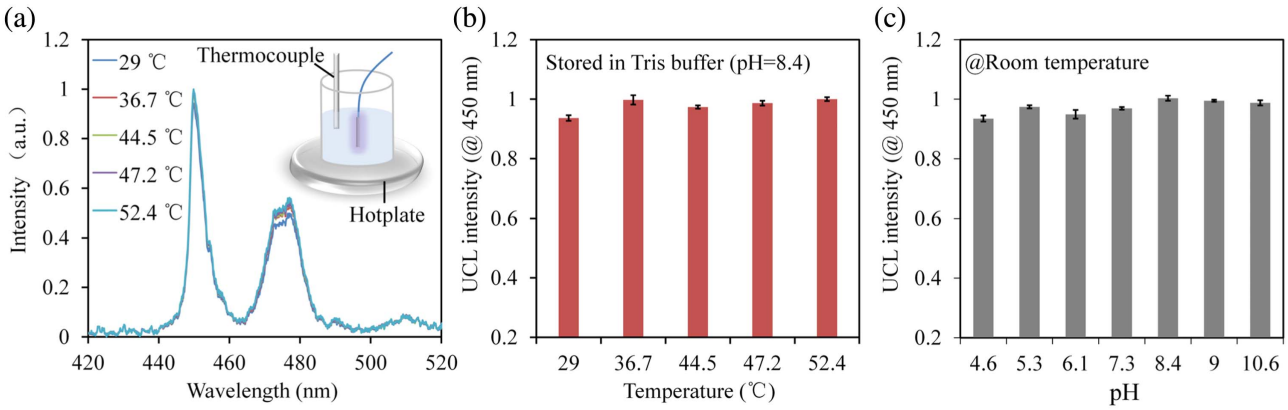

Fig. 3. (a) Dependence of the UCL spectrum on temperature. The inset image describes the corresponding experimental setup, where the sensor is immersed in a heating water bath (Tris-HCl buffer, pH = 8.4, ionic strength = 150 mM) and a thermocouple is employed for temperature calibration. (b) UCL intensities at 450 nm under different temperatures (Tris-HCl buffer, pH = 8.4, ionic strength = 150 mM). (c) UCL intensities at 450 nm under different pH values at room temperature.

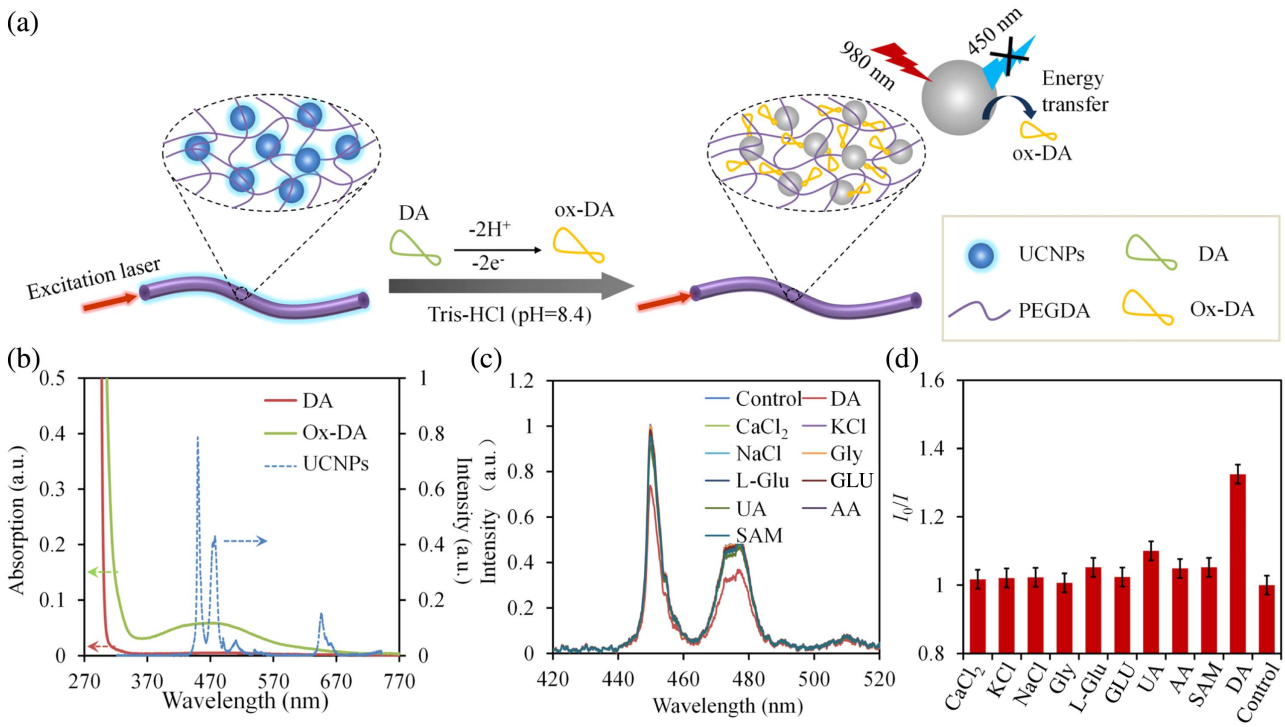

Fig. 4. (a) Mechanism of the UCNPs-HOF for DA sensing. (b) Absorption spectra of DA and ox-DA, and emission spectrum of the UCNPs-HOF. (c) Emission spectra of UCNPs-HOF immersed in different samples containing DA, $CaCl_2$, KCl, NaCl, glycine (Gly), L-glutamate (L-Glu), glucose (GLU), uric acid (UA), ascorbic acid (AA), and S-adenosylmetionine (SAM). The concentration of each sample is kept constant at 100 μM. (d) Selectivity of the UCNPs-HOF sensor.

As we have described in Fig. 3(c), the UCL intensity of UCNPs-HOF is insensitive to the changes of pH. It must be noted, however, that the spontaneous oxidation process of DA is highly pH-dependent. The oxidation process of DA in alkaline environment is more facile than that in acidic environment, resulting in higher efficiency of the UCL quenching at stronger alkaline pH [shown in Fig. 5(a)]. Therefore, for biological samples at different pH, calibration is required before DA testing. Figure 5(b) shows the response of the UCNPs-HOF sensor to various concentrations of DA. The quenching ratio of the sensor shows a linear relationship with the increasing concentration of DA in a range of 0–200 μM, demonstrating its capability in quantitative measurements [shown in Fig. 5(c)]. The quenching behaviors of the UCNPs-HOF sensor towards DA can be described in the form of the Stern–Volmer equation [22]:

$$I_0/I = K_{SV}[Q] + 1, \quad (1)$$

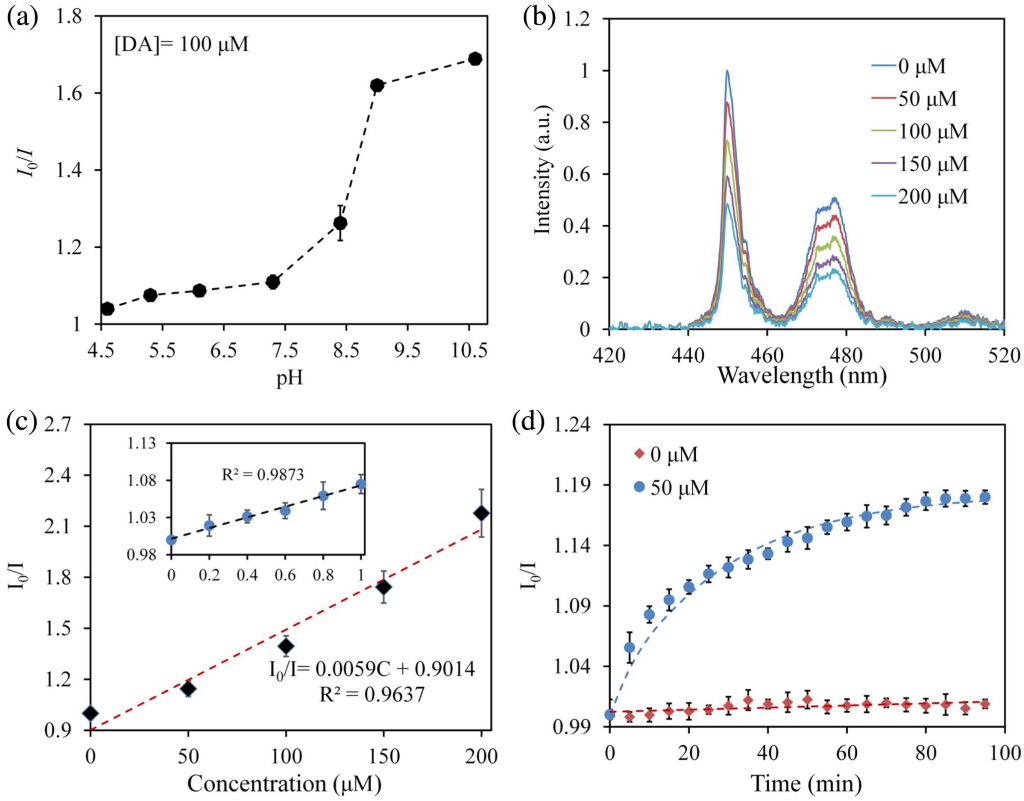

Fig. 5. (a) UCL quenching ratios of the UCNPs-HOF for DA sensing at different pH values. The DA concentration is set at 100 μM. (b) Emission spectra of the UCNPs-HOF versus the concentration of DA (Tris-HCl buffer, pH = 8.4, ionic strength = 150 mM). (c) Corresponding calibration curve of the UCNPs-HOF for DA detection in the range of 0–200 μM. Inset shows a linear plot in a small range of 0–1 μM. (d) Time response of the UCNPs-HOF sensor.

where I_0 and I are UCL intensities of the UCNPs-HOF in the absence and presence of DA, $[Q]$ is the concentration of the DA sample, and K_{SV} is the Stern–Volmer quenching constant. Following Eq. (1), the limit of detection (LOD) is calculated from three times the standard deviation divided by slope of the calibration slope (K_{SV}), which is estimated to be 83.6 nM, superior to that in other methods for DA detection [23,29,48,49]. The LOD of the sensor could be further enhanced by increasing the sample pH as a result of the higher quenching efficiency [shown in Fig. 5(a)]. The response time of the sensor is further investigated by continuously recording UCL spectra at a time interval of 5 min [shown in Fig. 5(d)]. In the absence of DA, the UCNPs-HOF in Tris-HCl buffer shows a stable readout for 100 min, with a maximal drift of 2.62%. With the addition of DA, the UCNPs-HOF shows immediate response and reaches saturation in 60 min as a result of sufficient accumulation of ox-DA, which suggests an optimal reaction time of ~60 min for DA detection. To further evaluate the practicality of the sensor for detecting DA in biofluids, human blood serum samples are tested. The detection of DA is conducted by spiking specified concentrations of DA with the human serum samples. The results are shown in Table 1. The recoveries of DA at the concentrations of 10, 30, and 50 μM are respectively 95%, 97%, and 104% with relative standard deviation (RSD) below 5%, which verifies the feasibility of the sensor for DA determination in real biological samples.

Table 1. Determination of DA in Samples of Human Blood Serum

Sample No.	Added (μM)	Measured (μM)	Recovery (%)	RSD (%, $n = 3$)
1	10	9.5	95	4.9
2	30	29.1	97	2.6
3	50	52.0	104	3.8

4. CONCLUSIONS

In summary, we have developed a soft and biocompatible optical DA sensor based on UCNPs-doped HOF. The UCNPs were synthesized with a core of $NaYF_4$:Yb, Tm and a shell of $NaYF_4$, which could generate visible UCL emissions at 450 nm upon NIR excitation. The HOF provided an implantable, biocompatible, and versatile platform for excitation and emission collection of the UCNPs, as well as analyte exchanging with the surrounding environments. DA molecules were quantified from UCL intensities at 450 nm through LET between UCNPs and oxidation products of DA. We showed that the UCNPs-HOF sensor was capable of accurately detecting DA in the range of 0–200 μM with high linearity, selectivity,

and sensitivity (LOD of 83.6 nM). The soft and biocompatible UCNPs-HOF sensor is expected to offer a promising point-of-care diagnostic tool for quantitative and *in situ* monitoring of DA in clinics.

Funding. National Natural Science Foundation of China (61805126); Tsinghua University Initiative Scientific Research Program (20193080076).

Acknowledgment. J. G. acknowledges funding from the National Natural Science Foundation of China (No. 61805126) and the Postdoctoral Innovation Talents Support Program. L. K. acknowledges the support from Tsinghua University Initiative Scientific Research Program (No. 20193080076).

L. K. and J. G. conceived the idea. B. Z. performed the experiments. J. G., B. Z., and L. K. analyzed the data. All authors contributed to the editing of the manuscript.

Disclosures. The authors declare no competing financial interest.

REFERENCES

1. N. X. Tritsch and B. L. Sabatini, "Dopaminergic modulation of synaptic transmission in cortex and striatum," Neuron **76**, 33–50 (2012).
2. N. D. Volkow, G. J. Wang, J. S. Fowler, D. Tomasi, F. Telang, and R. Baler, "Addiction: decreased reward sensitivity and increased expectation sensitivity conspire to overwhelm the brain's control circuit," Bioessays **32**, 748–755 (2010).
3. J. P. Kesby, D. W. Eyles, J. J. McGrath, and J. G. Scott, "Dopamine, psychosis and schizophrenia: the widening gap between basic and clinical neuroscience," Transl. Psychiatry **8**, 30 (2018).
4. P. Damier, E. C. Hirsch, Y. Agid, and A. M. Graybiel, "The substantia nigra of the human brain. II. Patterns of loss of dopamine-containing neurons in Parkinson's disease," Brain **122**, 1437–1448 (1999).
5. J. L. Eriksen, T. M. Dawson, D. W. Dickson, and L. Petrucelli, "Caught in the act: α-synuclein is the culprit in Parkinson's disease," Neuron **40**, 453–456 (2003).
6. X. Zhang, Q. Liu, Q. Liao, and Y. Zhao, "Potential roles of peripheral dopamine in tumor immunity," J. Cancer **8**, 2966–2973 (2017).
7. J. W. Tidey and K. A. Miczek, "Social defeat stress selectively alters mesocorticolimbic dopamine release: an *in vivo* microdialysis study," Brain Res. **721**, 140–149 (1996).
8. J. Chen, Y. P. Shi, and J. Y. Liu, "Determination of noradrenaline and dopamine in Chinese herbal extracts from *Portulaca oleracea* L. by high-performance liquid chromatography," J. Chromatogr. A **1003**, 127–132 (2003).
9. M. Li, J. E. Zhu, L. Zhang, X. Chen, H. Zhang, F. Zhang, S. Xu, and D. G. Evans, "Facile synthesis of NiAl-layered double hydroxide/graphene hybrid with enhanced electrochemical properties for detection of dopamine," Nanoscale **3**, 4240–4246 (2011).
10. C. Yang, E. Trikantzopoulos, M. D. Nguyen, C. B. Jacobs, Y. Wang, M. Mahjouri-Samani, I. N. Ivanov, and B. J. Venton, "Laser treated carbon nanotube yarn microelectrodes for rapid and sensitive detection of dopamine *in vivo*," ACS Sens. **1**, 508–515 (2016).
11. M. Ganesana, S. T. Lee, Y. Wang, and B. J. Venton, "Analytical techniques in neuroscience: recent advances in imaging, separation, and electrochemical methods," Anal. Chem. **89**, 314–341 (2017).
12. A. Roychoudhury, S. Basu, and S. K. Jha, "Dopamine biosensor based on surface functionalized nanostructured nickel oxide platform," Biosens. Bioelectron. **84**, 72–81 (2016).
13. A. Jaquins-Gerstl and A. C. Michael, "A review of the effects of FSCV and microdialysis measurements on dopamine release in the surrounding tissue," Analyst **140**, 3696–3708 (2015).
14. T. Patriarchi, J. R. Cho, K. Merten, M. W. Howe, A. Marley, W. H. Xiong, R. W. Folk, G. J. Broussard, R. Liang, M. L. Jang, H. Zhong, D. Dombeck, M. Zastrow, A. Nimmerjahn, V. Gradinaru, J. T. Williams, and L. Tian, "Ultrafast neuronal imaging of dopamine dynamics with designed genetically encoded sensors," Science **360**, eaat4422 (2018).
15. F. Sun, J. Zeng, M. Jing, J. Zhou, J. Feng, S. F. Owen, Y. Luo, F. Li, H. Wang, T. Yamaguchi, Z. Yong, Y. Gao, W. Peng, L. Wang, S. Zhang, J. Du, D. Lin, M. Xu, A. C. Kreiter, G. Cui, and Z. Yong, "A genetically encoded fluorescent sensor enables rapid and specific detection of dopamine in flies, fish, and mice," Cell **174**, 481–496 (2018).
16. K. Qu, J. Wang, J. Ren, and X. Qu, "Carbon dots prepared by hydrothermal treatment of dopamine as an effective fluorescent sensing platform for the label-free detection of iron (III) ions and dopamine," Chem. A Eur. J. **19**, 7243–7249 (2013).
17. Y. Tao, Y. Lin, J. Ren, and X. Qu, "A dual fluorometric and colorimetric sensor for dopamine based on BSA-stabilized aunanoclusters," Biosens. Bioelectron. **42**, 41–46 (2013).
18. A. Yildirim and M. Bayindir, "Turn-on fluorescent dopamine sensing based on in situ formation of visible light emitting polydopamine nanoparticles," Anal. Chem. **86**, 5508–5512 (2014).
19. I. L. Medintz, M. H. Stewart, S. A. Trammell, K. Susumu, J. B. Delehanty, B. C. Mei, J. S. Melinger, J. B. BlancoCanosa, P. E. Dawson, and H. Mattoussi, "Quantum-dot/dopamine bioconjugates function as redox coupled assemblies for in vitro and intracellular pH sensing," Nat. Mater. **9**, 676–684 (2010).
20. X. Zhang, X. Chen, S. Kai, H. Y. Wang, J. Yang, F. G. Wu, and Z. Chen, "Highly sensitive and selective detection of dopamine using one-pot synthesized highly photoluminescent silicon nanoparticles," Anal. Chem. **87**, 3360–3365 (2015).
21. Y. Ou, A. M. Buchanan, C. E. Witt, and P. Hashemi, "Frontiers in electrochemical sensors for neurotransmitter detection: towards measuring neurotransmitters as chemical diagnostics for brain disorders," Anal. Meth. **11**, 2738–2755 (2019).
22. B. Kumar, A. Murali, and S. Giri, "Upconversion nanoplatform for FRET-based sensing of dopamine and pH," ChemistrySelect **4**, 5407–5414 (2019).
23. B. Zhao and Y. Li, "Facile synthesis of near-infrared-excited $NaYF_4$:Yb^{3+}, Tm^{3+} nanoparticles for label-free detection of dopamine in biological fluids," Talanta **179**, 478–484 (2018).
24. X. Zhou, P. Ma, A. Wang, C. Yu, T. Qian, S. Wu, and J. Shen, "Dopamine fluorescent sensors based on polypyrrole/graphene quantum dots core/shell hybrids," Biosens. Bioelectron. **64**, 404–410 (2015).
25. J. Zhao, L. Zhao, C. Lan, and S. Zhao, "Graphene quantum dots as effective probes for label-free fluorescence detection of dopamine," Sens. Actuat. B **223**, 246–251 (2016).
26. A. Pathak and B. D. Gupta, "Ultra-selective fiber optic SPR platform for the sensing of dopamine in synthetic cerebrospinal fluid incorporating permselective nafion membrane and surface imprinted MWCNTs-PPy matrix," Biosens. Bioelectron. **133**, 205–214 (2019).
27. N. Agrawal, B. Zhang, C. Saha, C. Kumar, B. K. Kaushik, and S. Kumar, "Development of dopamine sensor using silver nanoparticles and PEG-functionalized tapered optical fiber structure," IEEE Trans. Biomed. Eng. **76**, 1542–1547 (2019).
28. D. R. Raj, S. Prasanth, T. V. Vineeshkumar, and C. Sudarsanakumar, "Surface plasmon resonance based fiber optic dopamine sensor using green synthesized silver nanoparticles," Sens. Actuat. B **224**, 600–606 (2016).
29. M. H. Kim, H. Yoon, S. H. Choi, F. Zhao, J. Kim, K. D. Song, and U. Lee, "Miniaturized and wireless optical neurotransmitter sensor for real-time monitoring of dopamine in the brain," Sensors **16**, 1894 (2016).
30. S. Baluta, J. Cabaj, and K. Malecha, "Neurotransmitters detection using a fluorescence-based sensor with graphene quantum dots," Opt. Appl. **47**, 225–231 (2017).
31. S. Shabahang, S. Kim, and S. H. Yun, "Light-guiding biomaterials for biomedical applications," Adv. Funct. Mater. **28**, 1706635 (2018).
32. L. Wang, C. Zhong, D. Ke, F. Ye, J. Tu, L. Wang, and Y. Lu, "Ultrasoft and highly stretchable hydrogel optical fibers for *in vivo* optogenetic modulations," Adv. Opt. Mater. **6**, 1800427 (2018).

33. N. Jiang, R. Ahmed, A. A. Rifat, J. Guo, Y. Yin, Y. Montelongo, H. Butt, and A. K. Yetisen, "Functionalized flexible soft polymer optical fibers for laser photomedicine," Adv. Opt. Mater. **6**, 1701118 (2018).
34. J. Guo, M. Niu, and C. Yang, "Highly flexible and stretchable optical strain sensing for human motion detection," Optica **4**, 1285–1288 (2017).
35. J. Guo, X. Liu, N. Jiang, A. K. Yetisen, H. Yuk, C. Yang, A. Khademhosseini, X. Zhao, and S. H. Yun, "Highly stretchable, strain sensing hydrogel optical fibers," Adv. Mater. **28**, 10244–10249 (2016).
36. J. Guo, B. Zhou, C. Yang, Q. Dai, and L. Kong, "Stretchable and temperature-sensitive polymer optical fibers for wearable health monitoring," Adv. Funct. Mater. **29**, 1902898 (2019).
37. A. K. Yetisen, N. Jiang, A. Fallahi, Y. Montelongo, G. U. Ruiz-Esparza, A. Tamayol, Y. S. Zhang, I. Mahmood, S. Yang, K. S. Kim, H. Butt, A. Khademhosseini, and S. Yun, "Glucose-sensitive hydrogel optical fibers functionalized with phenylboronic acid," Adv. Mater. **29**, 1606380 (2017).
38. J. Guo, H. Huang, M. Zhou, C. Yang, and L. Kong, "Quantum dots-doped tapered hydrogel waveguide for ratiometric sensing of metal ions," Anal. Chem. **90**, 12292–12298 (2018).
39. M. Zhou, J. Guo, and C. Yang, "Ratiometric fluorescence sensor for Fe^{3+} ions detection based on quantum dot-doped hydrogel optical fiber," Sens. Actuat. B **264**, 52–58 (2018).
40. M. Choi, J. W. Choi, S. Kim, S. Nizamoglu, S. K. Hahn, and S. H. Yun, "Light-guiding hydrogels for cell-based sensing and optogenetic synthesis *in vivo*," Nat. Photonics **7**, 987–994 (2013).
41. S. Nizamoglu, M. C. Gather, M. Humar, M. Choi, S. Kim, K. S. Kim, S. K. Hahn, G. Scarcelli, M. Randolph, R. W. Redmond, and S. H. Yun, "Bioabsorbable polymer optical waveguides for deep-tissue photomedicine," Nat. Commun. **7**, 10374 (2016).
42. H. Sheng, X. Wang, N. Kong, W. Xi, H. Yang, X. Wu, K. Wu, C. Li, J. Hu, J. Tang, J. Zhou, S. Duan, H. Wang, and Z. Suo, "Neural interfaces by hydrogels," Extreme Mech. Lett. **30**, 100510 (2019).
43. X. Zhao, "EML webinar overview: extreme mechanics of soft materials for merging human-machine intelligence," Extreme Mech. Lett. **39**, 100784 (2020).
44. G. S. Yi and G. M. Chow, "Water-soluble $NaYF_4$:Yb, Er (Tm)/$NaYF_4$/polymer core/shell/shell nanoparticles with significant enhancement of upconversion fluorescence," Chem. Mater. **19**, 341–343 (2007).
45. J. Guo, B. Zhou, C. Yang, Q. Dai, and L. Kong, "Stretchable and upconversion-luminescent polymeric optical sensor for wearable multifunctional sensing," Opt. Lett. **44**, 5747–5750 (2019).
46. G. C. Le Goff, R. L. Srinivas, W. A. Hill, and P. S. Doyle, "Hydrogel microparticles for biosensing," Eur. Polym. J. **72**, 386–412 (2015).
47. A. S. Hoffman, "Hydrogels for biomedical applications," Adv. Drug Delivery Rev. **64**, 18–23 (2012).
48. X. Cao, X. L. Cai, and N. Wang, "Selective sensing of dopamine at MnOOH nanobelt modified electrode," Sens. Actuat. B **160**, 771–776 (2011).
49. J. J. Zhao, L. M. Zhao, C. Q. Lan, and S. L. Zhao, "Graphene quantum dots as effective probes for label-free fluorescence detection of dopamine," Sens. Actuat. B **223**, 246–251 (2016).